Journal of Electroanalytical Chemistry 936 (2023) 117357

Contents lists available at ScienceDirect

Journal of Electroanalytical Chemistry

journal homepage: www.elsevier.com/locate/jelechem

Stable zinc metal anode with an ultrathin carbon coating for zinc-ion batteries

Xiaolin Zhang, Qingdong Ruan, Liangliang Liu, Dan Li, Yue Xu, Yinchuan Wang, Jinyuan Liu, Chao Huang, Fangyu Xiong *, Bin Wang *, Paul K Chu *

Department of Physics, Department of Materials Science and Engineering, and Department of Biomedical Engineering, City University of Hong Kong, Tat Chee Avenue, Kowloon, Hong Kong, China

ARTICLE INFO

Keywords:
Carbon coating
Zinc metal anode
Zinc-ion battery
Surface modification

ABSTRACT

Owing to the good safety, low cost, environmentally friendliness, and relatively high energy density, aqueous zinc-ion batteries (ZIBs) are promising alternatives to lithium-ion batteries. However, the zinc metal anode in aqueous ZIBs is prone to dendrite growth and side reactions. Herein, an ultrathin carbon coating is fabricated on the Zn metal anode to suppress dendrite growth and alleviate side reactions. The symmetrical cell containing the modified Zn electrode shows a long cycling life of 3500 h at 0.5, 1 and 2 mA cm^{-2} with areal capacities of 0.5, 1 and 2 mAh cm^{-2}, respectively. The cycling life is superior to those of previously reported Zn metal anodes with carbon-based coatings. Meanwhile, the full ZIB using Zn anode with ultrathin carbon coating deliver enhanced rate performance and cycling stability compared to that of using bare Zn anode.

1. Introduction

Lithium-ion batteries (LIBs) are widely used in portable electronics, electric vehicles, and energy storage stations [1–3]. However, accidents arising from combustion of the flammable organic liquid electrolytes are quite common for electric vehicles and energy storage stations [4–6]. In this respect, aqueous zinc-ion batteries (ZIBs) have attracted increasing attention due to the better safety and non-flammable aqueous electrolytes [7–10]. Moreover, Zn with a high theoretical capacity (5855 mAh cm^{-3} and 820 mAh g^{-1}) and suitable redox potential of − 0.76 V (vs standard hydrogen electrode) is a desirable anode for aqueous high-energy–density ZIBs [10–13]. However, Zn metal anodes are vulnerable to dendrite growth in the hydrogen evolution reaction (HER) as well as Zn corrosion resulting in early failure of aqueous ZIBs comprising Zn metal anodes [13–15].

Many strategies have been proposed to overcome these shortcomings, for instance, electrolyte regulation, host design, and surface modification [12–21]. In particular, depositing a surface coating on Zn metal is a simple and efficient way [15–17] to mitigate undesirable side reactions by isolating the Zn anode from the electrolyte and suppress Zn dendrite growth by improving the surface wettability and homogenizing the electric field [15,16,22–26]. Carbon-based materials are desirable coatings for Zn metal anodes due to the high electrical conductivity, chemical stability, and abundant resource [16,27,28]. Recently, some carbonaceous materials including graphite [29], active carbon [30], graphene [31–33], and graphdiyne [34] have been proposed for Zn metal anodes to improve the electrochemical properties. However, most of these carbon-based coatings are quite thick consequently compressing the energy density and increasing the interfacial charge transfer resistance [30,33,35–37]. Hence, ultrathin carbon-based coatings may deliver better performance for ZIBs but related research has been rare [32].

Herein, Zn metal with ultrathin carbon coatings (C@Zn) is prepared by magnetron sputtering as stable anodes in ZIBs. The carbon coating increases the surface wettability, enables more uniform Zn plating, and mitigates undesirable side reactions. The symmetrical cell composed of the C@Zn anode exhibits enhanced plating/stripping stability of 3,500 h and reduced voltage hysteresis compared to the bare Zn symmetrical cell. In addition, the full ZIB with the C@Zn anode has higher rate and cycling capability suggesting large potential in commercial application.

2. Experimental section

2.1. Synthesis of C@Zn anodes

The Zn foil with a thickness of 0.1 mm was cut into disks with a diameter of 12 mm and polished with 2,000 mesh sandpaper. Carbon coatings were deposited on the Zn samples by magnetron sputtering

* Corresponding authors.
E-mail addresses: fxiong@cityu.edu.hk (F. Xiong), bwang63@cityu.edu.hk (B. Wang), paul.chu@cityu.edu.hk (P.K Chu).

https://doi.org/10.1016/j.jelechem.2023.117357
Received 25 January 2023; Received in revised form 14 March 2023; Accepted 16 March 2023
Available online 20 March 2023

using a graphite target and Ar as the sputtering gas. Direct-current pulses with a power of 100 W were applied to the substrate and the pressure in the vacuum chamber was 0.5 Pa. The C@Zn anodes prepared with sputtering time of 30, 60, and 90 min are denoted as C@Zn-1, C@Zn-2 and C@Zn-3, respectively.

2.2. Synthesis of $Mg_xV_2O_5{\cdot}nH_2O$ cathodes

The $Mg_xV_2O_5{\cdot}nH_2O$ cathodes were prepared by mixing 70 % $Mg_xV_2O_5{\cdot}nH_2O$ powders, 30 % acetylene black, and 10 % polytetrafluoroethylene (PTFE). The $Mg_xV_2O_5{\cdot}nH_2O$ powder was synthesized by a hydrothermal method. 0.545 g of V_2O_5 were dissolved in 24 mL of deionized water and stirred for 10 min. 6 mL of H_2O_2 (30.0 %) were introduced and stirred for 10 min to obtain a reddish-brown solution. Afterwards, 0.203 g $MgCl_2{\cdot}6H_2O$ were added, stirred for 10 min, placed in a 50 mL Teflon-lined sealed autoclave, and heated to 200 °C for 48 h. After cooling to room temperature, the precipitate was collected by centrifugation, washed with deionized water and ethanol, and dried at 70 °C to obtain the $Mg_xV_2O_5{\cdot}nH_2O$ powder.

2.3. Materials characterization

X-ray diffraction (XRD) was carried out on the Rigaku Smartlab X-ray diffractometer using Cu K_α radiation and the Raman spectra were obtained on the LabRAM HR800 laser confocal micro-Raman spectrometer at a laser wavelength of 514.5 nm. The thickness of the carbon coatings was determined on the Bruker DektakXT profilometer. Scanning electron microscopy (SEM) and energy-dispersive X-ray spectroscopy (EDS) were conducted on the Thermo Fisher QUATTRO S and the surface contact angles were measured using the Ramé-Hart instrument (USA).

2.4. Electrochemical measurements

The electrochemical properties were determined from CR2016 coin cells with 2 M $ZnSO_4$ aqueous solution as the electrolyte and glass fiber filter (GF/D Whatman) as the separator. In the symmetrical cells, the bare Zn, C@Zn-1, C@Zn-2, or C@Zn-3 were used as both the cathode and anode, whereas the full cells are composed of the $Mg_xV_2O_5{\cdot}nH_2O$ cathode and bare Zn or C@Zn-3 anode. Galvanostatic charging/discharging was carried out on the Neware battery test system (CT-4008) at room temperature. Linear scan voltammetry (LSV), Tafel polarization, cyclic voltammetry (CV), and electrochemical impedance spectroscopy (EIS) were conducted on an electrochemical workstation (CHI 660E).

3. Results and discussion

The XRD patterns of bare Zn, C@Zn-1, C@Zn-2, and C@Zn-3 (Fig. 1**a**) match those of zinc metal (JCPDS No. 04–0831) but no carbon signals are detected because the carbon coatings are very thin and amorphous. As shown in Fig. 1**b**, no Raman band appears in the range of 1000 to 2000 cm^{-1} from bare Zn, but a broad band spanning 1300 to 1700 cm^{-1} is observed from the Raman scattering spectra of C@Zn-1, C@Zn-2, and C@Zn-3. This broad band is a combination of the D and G bands of carbonaceous materials [29,38,39]. The detailed analysis discloses that the G band is more intense than the D band indica-

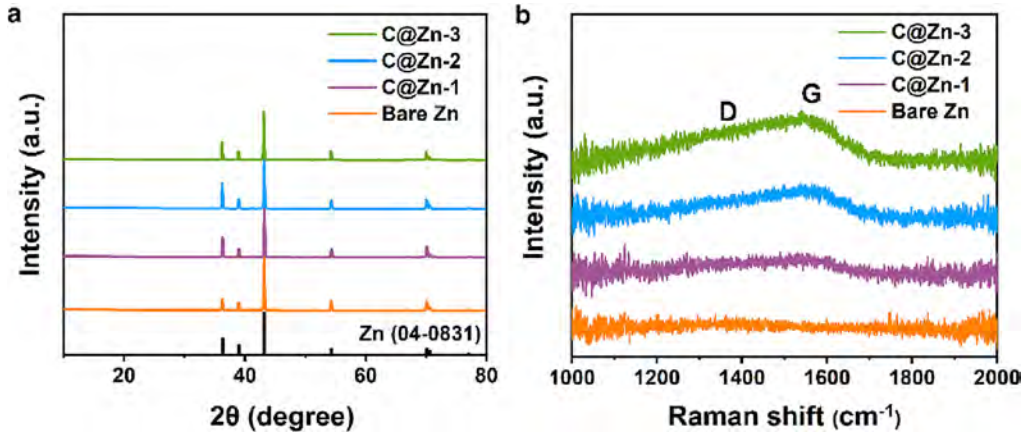

Fig. 1. (a) XRD patterns and (b) Raman scattering spectra of bare Zn, C@Zn-1, C@Zn-2, and C@Zn-3.

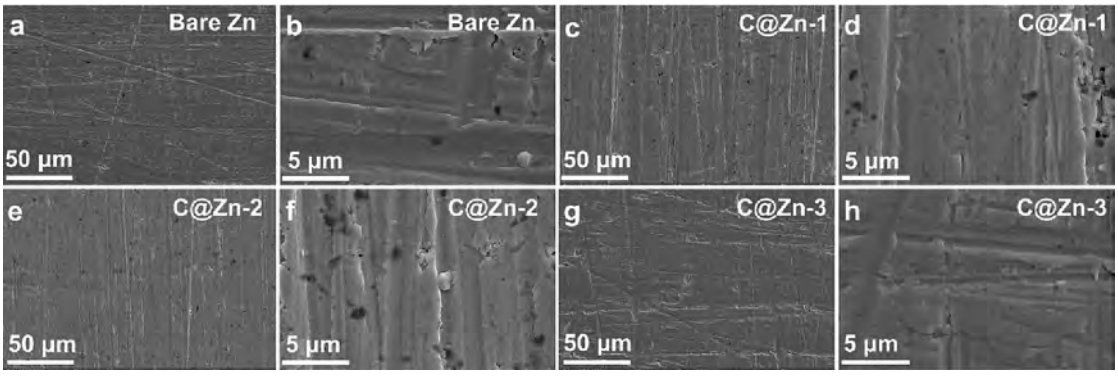

Fig. 2. SEM images of (a, b) Bare Zn, (c, d) C@Zn-1, (e, f) C@Zn-2, and (g, h) C@Zn-3.

tive of a high degree of graphitization which improves the electrical conductivity and charge dispersion on the Zn anode. The intensity of this band increases from C@Zn-1 to C@Zn-2 to C@Zn-3 with increasing thickness, which is also reflected by the color change (Fig. S2). The Zn samples become darker as the carbon layers become thicker. To determine the thickness of the carbon coatings, carbon coatings are

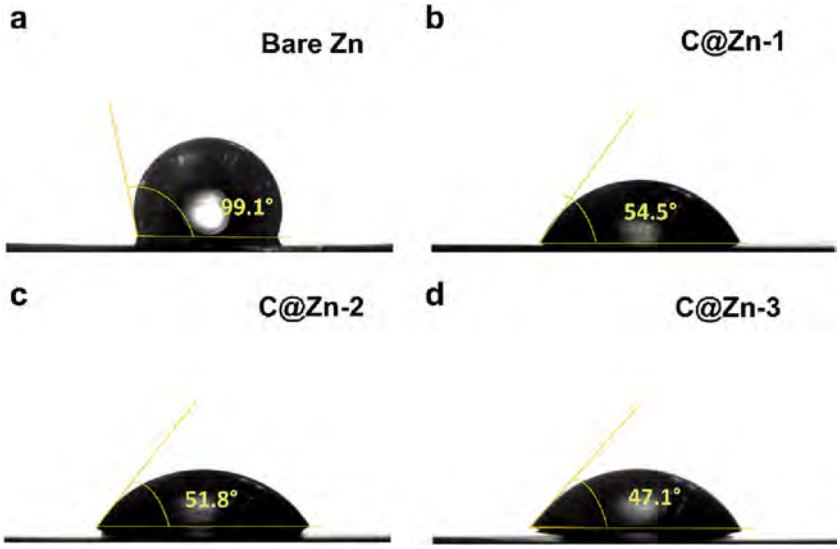

Fig. 3. Deionized water contact angles: (a) Bare Zn, (b) C@Zn-1, (c) C@Zn-2, and (d) C@Zn-3.

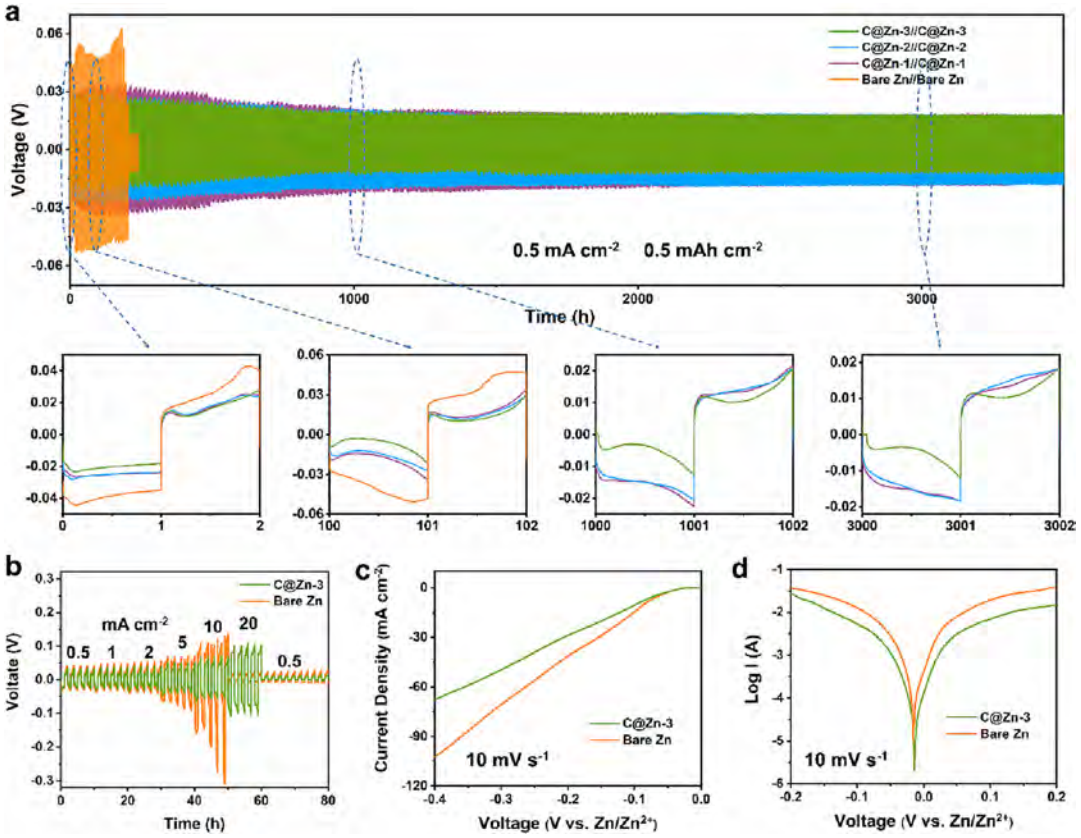

Fig. 4. (a) Voltage profiles of the bare Zn, C@Zn-1, C@Zn-2, and C@Zn-3 symmetrical cells cycling at 0.5 mA cm^{-2} with an areal capacity of 0.5 mAh cm^{-2}; (b) Rate performance of the bare Zn and C@Zn-3 symmetrical cells (bare Zn: from 0.5 to 10 mA cm^{-2}; C@Zn-3: from 0.5 to 20 mA cm^{-2}). (c) LSV curves and (d) Tafel plots of bare Zn and C@Zn-3 at 10 mV s^{-1}.

deposited on a partially masked Si substrate (**Fig. S1**) and profilometry reveals that the thicknesses of the 30, 60 and 90-min coatings are about 6, 12 and 20 nm, respectively.

The SEM images of the bare Zn (Fig. 2**a, b**) show a flat surface with some scratches from polishing and the SEM images of C@Zn-1, C@Zn-2, and C@Zn-3 (Fig. 2**c-h**) display similar results, indicating that the thin carbon coatings do not alter the surface morphology.

The contact angles are determined (Fig. 3) and the bare Zn without a carbon coating shows a large contact angle of 99.1° (Fig. 3**a**) implying poor hydrophilicity and surface wettability. In contrast, C@Zn-1, C@Zn-2, and C@Zn-3 exhibit smaller contact angles of 54.5°, 51.8° and 47.1° (Fig. 3**b-d**), respectively, for higher hydrophilicity and surface wettability, which facilitate interfacial charge transfer on the Zn metal anode in aqueous ZIBs [23,24,40].

To demonstrate the effects of the ultrathin carbon coatings on the electrochemical properties of the Zn metal anode, symmetrical cells are assembled to evaluate the plating/stripping stability of bare Zn, C@Zn-1, C@Zn-2, and C@Zn-3. During cycling at 0.5 mA cm^{-2} with an areal capacity of 0.5 mAh cm^{-2}, the voltage of the bare Zn symmetrical cell drops abruptly to nearly zero after about 200 h indicative of a short circuit (Fig. 4**a**). In comparison, the C@Zn-1, C@Zn-2, and C@Zn-3 symmetrical cells operate stably for 3,500 h with enhanced plating/stripping stability. Moreover, the C@Zn-1, C@Zn-2, and C@Zn-3 symmetrical cells exhibit reduced voltage hysteresis compared to the bare Zn symmetrical cell and in particular, the C@Zn-3 symmetrical cell shows the lowest voltage hysteresis. Therefore, C@Zn-3 is chosen to in the subsequent investigation. Even at higher current densities of 1 mA cm^{-2} and 2 mA cm^{-2} with areal capacities of 1 mAh cm^{-2} and 2 mAh cm^{-2}, respectively, the C@Zn-3 symmetrical cell still has a long cycling life of 3,500 h (**Fig. S3 and S4**), which is longer than that of recently reported Zn anodes with carbon-based coatings [29,30,32–37]. The rate characteristics of the bare Zn and C@Zn-3 symmetrical cells are evaluated by galvanostatic charging-discharging at different current densities for a constant plating/stripping time of 1 h (Fig. 4**b**). Compared to the bare Zn symmetrical cell, the C@Zn-3 symmetrical cell exhibits lower voltage hysteresis at all current densities and better Zn plating/stripping. Furthermore, the LSV curves (Fig. 4**c**) show that the HER current of the C@Zn-3 anode at − 0.2 V (vs Zn^{2+}/Zn) is lower than that of the bare Zn and the Tafel plot of C@Zn-3 (Fig. 4**d**) discloses higher corrosion potential and lower corrosion current due to the ultrathin carbon coating. In addition, the electrochemical characteristics of the Zn//Cu batteries are evaluated to confirm the protective effects of the carbon coating. The Cu electrode with the carbon coating (denoted as C@Cu-3) is pre-

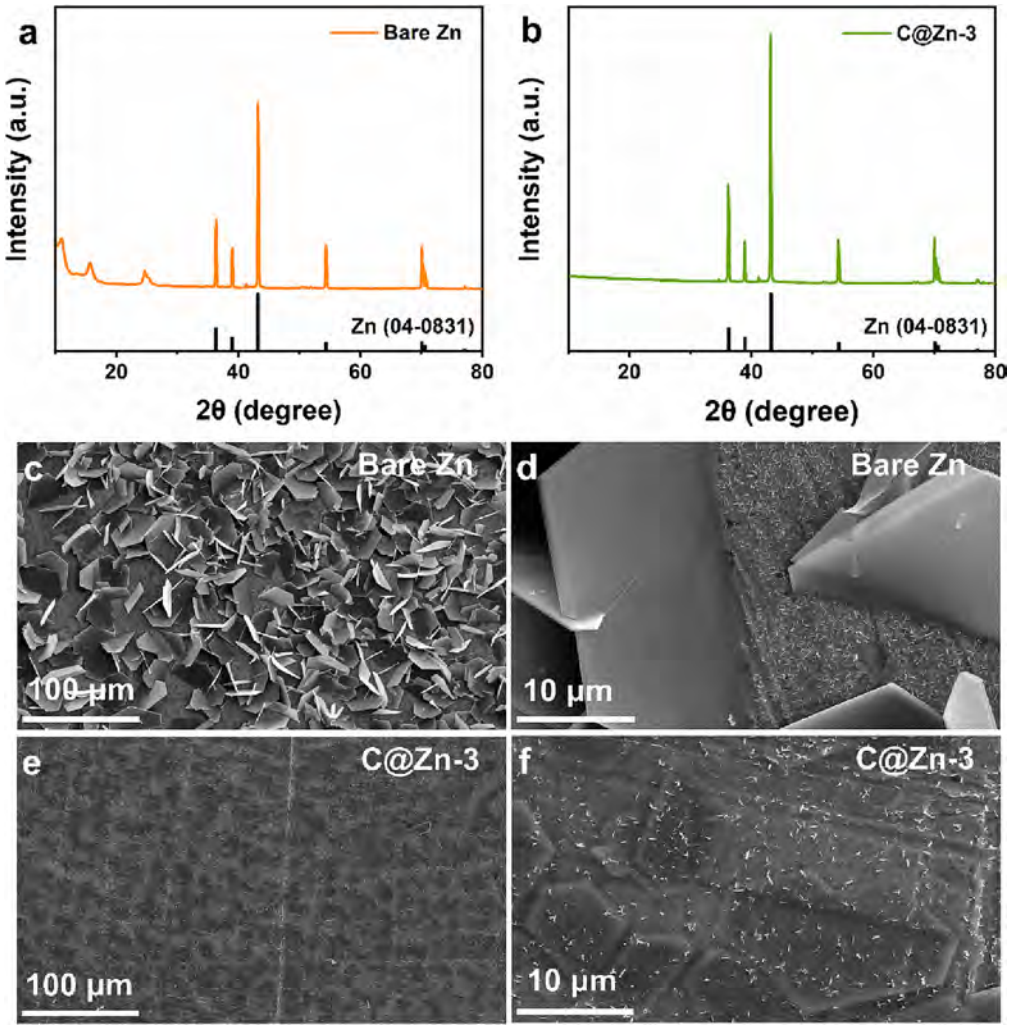

Fig. 5. XRD patterns of (a) bare Zn and (b) C@Zn-3 anodes after soaking in 2 M $ZnSO_4$ electrolyte for 3 days; SEM images of (c, d) bare Zn and (e, f) C@Zn-3 anodes after soaking in 2 M $ZnSO_4$ electrolyte for 3 days.

pared by a protocol similar to that of C@Zn-3. Compared to the bare Zn//bare Cu cell, the C@Zu-3//C@Cu-3 cell shows higher Coulombic efficiency during cycling (Fig. S5) providing evidence that the carbon coating indeed alleviates the side reactions.

In order to clarify the protective effects of the carbon coatings, the bare Zn and C@Zn-3 anodes are characterized after soaking in 2 M $ZnSO_4$ for 3 days. As shown in the XRD pattern of the bare Zn after soaking (Fig. 5**a**), the other diffraction peaks are derived from by-products in HER and Zn corrosion in the $ZnSO_4$ electrolyte, for example, $Zn_4SO_4(OH)_6{\cdot}xH_2O$ [41–43]. In contrast, no obvious by-product diffraction peaks are observed from C@Zn-3 after soaking (Fig. 5**b**) thus providing evidence that corrosion of C@Zn-3 is inhibited by the carbon coating. In addition, the SEM images (Fig. 5**c, d**) show that sheet-like by-products appear from the surface of the bare Zn after soaking and EDS reveals that they contain $Zn_4SO_4(OH)_6{\cdot}xH_2O$ (**Fig. S6a, b**) consistent with XRD. In comparison, only few sheet-like structures can be observed from the surface of C@Zn-3 after soaking (Fig. 5**e, f**) and most of the sheets are beneath the carbon coating and parallel to the surface. The EDS spectrum of the soaked C@Zn-3 shows weaker S signals than the bare Zn (**Fig. S6**). These results indicate that the carbon coating suppresses Zn corrosion by preventing direct contact between the electrolyte and Zn anode. Moreover, the diffraction peaks of the by-product ($Zn_4SO_4(OH)_6{\cdot}xH_2O$) are intense in the XRD pattern of the cycled bare Zn anode but weaker peaks are observed from the cycled C@Zn-3 anode (**Fig. S7**). The results demonstrate that the side reactions are hindered by the carbon coating during Zn plating/stripping.

The morphology of bare Zn and C@Zn-3 after Zn plating at 0.5 mA cm^{-2} for 1 h is examined and the SEM image (Fig. 6**a**) shows that the plated Zn on the bare Zn is loose and composed of nanosheets. Moreover, the distribution of plated Zn on the surface of the bare Zn is uneven (Fig. 6**b**), which may exacerbate the growth of Zn dendrites and increases the chance of short circuit in the battery during repeated Zn plating/stripping. In contrast, C@Zn-3 after Zn plating shows a flatter surface (Fig. 6**c, d**) and more uniform Zn plating, which is responsible for the excellent stability of Zn plating/stripping of C@Zn-3. The uniform Zn plating is attributed to the better surface wettability and more uniform charge distribution resulting from the carbon coating. The Zn nanosheets can be seen to be beneath the carbon coating from areas where the coating is broken (**Fig. S8**) verifying that the carbon coating play a protective role in the whole plating/stripping process.

To further evaluate the potential of the C@Zn-3 anode in practice, full cells are assembled with C@Zn-3 as the anode and $Mg_xV_2O_5{\cdot}nH_2O$ as the cathode (denoted as C@Zn-3//MgVO). The XRD pattern of the cathode (**Fig. S9**) matches that of previously reported $Mg_xV_2O_5{\cdot}nH_2O$ [44] and EDS shows the presence of Mg, V, and O in the cathode (**Fig. S10**), demonstrating successful synthesis of $Mg_xV_2O_5{\cdot}nH_2O$. The SEM images (**Fig. S11**) show that $Mg_xV_2O_5{\cdot}nH_2O$ is composed of microparticles. The CV curves of the C@Zn-3//MgVO and bare Zn//MgVO full cells in the voltage range of 0.3–1.6 V show similar redox peaks and similar reactions (Fig. 7**a**). The CV curve of the C@Zn-3//MgVO full cell has a larger area and slightly smaller polarization voltage than the bare Zn//MgVO full cell, indicating higher capacity and faster reaction kinetics. In addition, the C@Zn-3//MgVO full cell delivers better rate performance than the bare Zn//MgVO battery (Fig. 7**b**). The average discharge capacities of the C@Zn-3//MgVO full cell are 320.5, 255.5, 206.3, 138.2, and 84.5 mAh g^{-1} at 0.5, 1, 2, 5, and 10 A g^{-1}, respectively. In comparison, the bare Zn//MgVO full cell has lower average discharge capacities of 286.8, 227.2, 172.1, 101.3, and 56.6 mAh g^{-1} at 0.5, 1, 2, 5, and 10 A g^{-1}, respectively. The charging/discharging curves of the C@Zn-3//MgVO and bare Zn//MgVO full cells for different current densities are displayed in Fig. 7**c, d** which show that the C@Zn-3//MgVO full cell has a smaller overpotential, especially at high current densities due to enhanced Zn plating/stripping kinetics on the C@Zn-3 anode. The EIS plots are depicted in **Fig. S12** and compared to the bare Zn//MgVO battery, the C@Zn-3//MgVO full cell exhibits a smaller semicircle in the high frequency region and smaller interfacial charge transfer resistance. The long-term cycling stability is evaluated at a current density of 5 A g^{-1} (Fig. 7**e**). After 3,000 cycles, the capacity of the C@Zn-3//MgVO full cell is 112.5 mAh g^{-1}, which is higher than that of the bare Zn//MgVO full cell (88.4 mAh g^{-1}). The electrochemical results confirm the superiority of the C@Zn-3 anode boding well for commercial adoption.

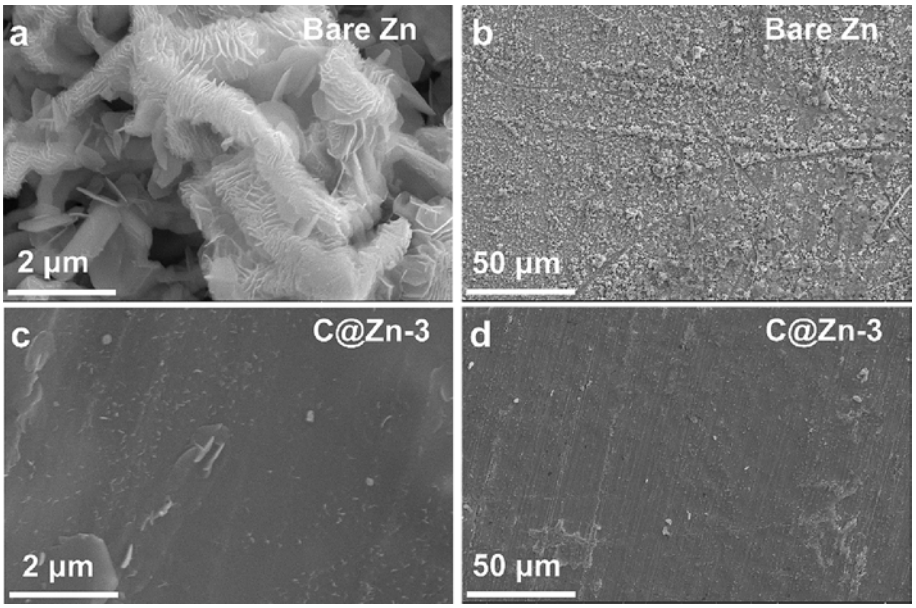

Fig. 6. SEM images of (a, b) bare Zn and (c, d) C@Zn-3 anodes after Zn plating at 0.5 mA cm^{-2} for 1 h.

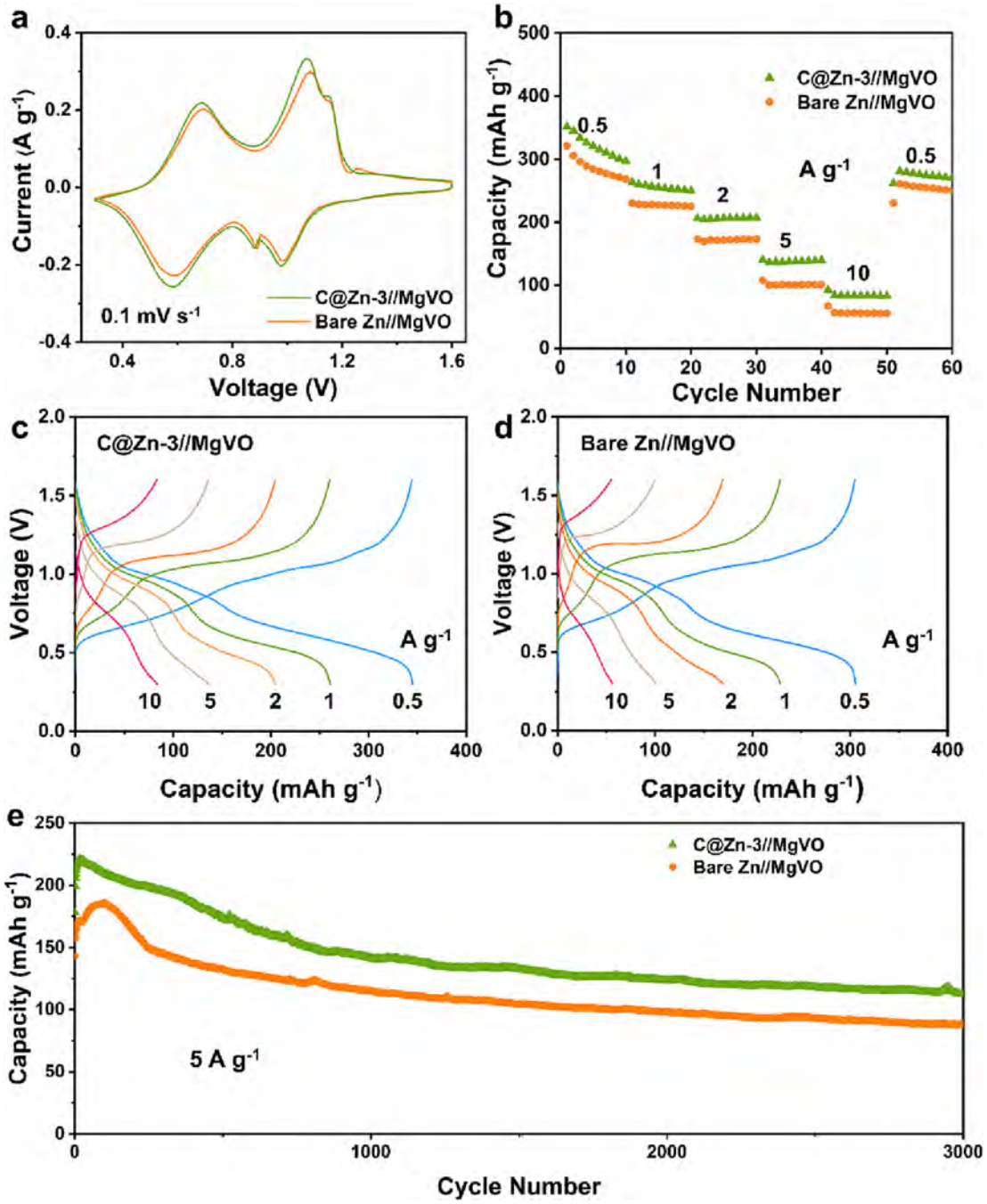

Fig. 7. (a) CV curves of the C@Zn-3//MgVO and bare Zn//MgVO full cells at 0.1 mV s^{-1} and 3rd cycle; (b) Rate performance of the C@Zn-3//MgVO and bare Zn//MgVO full cells; Charging/discharging curves of (c) C@Zn-3//MgVO and (d) Bare Zn//MgVO batteries at different current densities; (e) Cycling characteristics of the C@Zn-3//MgVO and bare Zn//MgVO full cells at 5 g^{-1}.

4. Conclusion

The Zn metal anode is coated with an ultrathin carbon layer to enhance the properties and stability of zinc-ion batteries (ZIBs). The carbon coating isolates the Zn metal from the electrolyte and improves the hydrophilicity, surface wettability, corrosion resistance, and Zn plating uniformity. The C@Zn-3 anode exhibits a long cycling life of 3,500 h in the symmetrical cell at current densities of 0.5, 1, and 2 mA cm^{-2} with areal capacities of 0.5, 1 and 2 mAh cm^{-2}, respectively. The C@Zn-3//MgVO full cell also shows enhanced rate characteristics (138.2 and 84.5 mAh g^{-1} at 5 and 10 A g^{-1}, respectively) and cycling stability (112.5 mAh g^{-1} after 3,000 cycles at 5 A g^{-1}). The results reveal that deposition of an ultrathin coating on Zn anodes is an effective means to improve the properties and stability of ZIBs and the technique has commercial potential.

Declaration of Competing Interest

The authors declare that they have no known competing financial interests or personal relationships that could have appeared to influence the work reported in this paper.

Acknowledgements

The work was supported by City University of Hong Kong Strategic Research Grant (SRG No. 7005505), City University of Hong Kong Donation Research Grant (DON-RMG No. 9229021), as well as Hong Kong Scholars Program (No. XJ2021021).

Appendix A. Supplementary data

Supplementary data to this article can be found online at https://doi.org/10.1016/j.jelechem.2023.117357.

References

[1] L.-Z. Fan, H. He, C.-W. Nan, Tailoring inorganic–polymer composites for the mass production of solid-state batteries, Nat. Rev. Mater. 6 (2021) 1003–1019, https://doi.org/10.1038/s41578-021-00320-0.
[2] Y. Liang, H. Dong, D. Aurbach, Y. Yao, Current status and future directions of multivalent metal-ion batteries, Nat. Energy 5 (2020) 646–656, https://doi.org/10.1038/s41560-020-0655-0.
[3] F. Xiong, S. Tan, X. Yao, Q. An, L. Mai, Crystal defect modulation in cathode materials for non-lithium ion batteries: Progress and challenges, Mater. Today 45 (2021) 169–190, https://doi.org/10.1016/j.mattod.2020.12.002.
[4] Y. Zheng, Y. Yao, J. Ou, M. Li, D. Luo, H. Dou, Z. Li, K. Amine, A. Yu, Z. Chen, A review of composite solid-state electrolytes for lithium batteries: fundamentals, key materials and advanced structures, Chem. Soc. Rev. 49 (2020) 8790–8839, https://doi.org/10.1039/d0cs00305k.
[5] T. Famprikis, P. Canepa, J.A. Dawson, M.S. Islam, C. Masquelier, Fundamentals of inorganic solid-state electrolytes for batteries, Nat. Mater. 18 (2019) 1278–1291, https://doi.org/10.1038/s41563-019-0431-3.
[6] D. Chao, W. Zhou, F. Xie, C. Ye, H. Li, M. Jaroniec, S.Z. Qiao, Roadmap for advanced aqueous batteries: From design of materials to applications, Sci. Adv., 6 (2020) eaba4098. https://doi.org/10.1126/sciadv.aba4098.
[7] C. Li, S. Jin, L.A. Archer, L.F. Nazar, Toward practical aqueous zinc-ion batteries for electrochemical energy storage, Joule 6 (2022) 1733–1738, https://doi.org/10.1016/j.joule.2022.06.002.
[8] H. Li, L. Ma, C. Han, Z. Wang, Z. Liu, Z. Tang, C. Zhi, Advanced rechargeable zinc-based batteries: Recent progress and future perspectives, Nano Energy 62 (2019) 550–587, https://doi.org/10.1016/j.nanoen.2019.05.059.
[9] G. Fang, J. Zhou, A. Pan, S. Liang, Recent Advances in Aqueous Zinc-Ion Batteries, ACS Energy Lett. 3 (2018) 2480–2501, https://doi.org/10.1021/acsenergylett.8b01426.
[10] M. Song, H. Tan, D. Chao, H.J. Fan, Recent Advances in Zn-Ion Batteries, Adv. Funct. Mater. 28 (2018) 1802564, https://doi.org/10.1002/adfm.201802564.
[11] X. Zeng, J. Liu, J. Mao, J. Hao, Z. Wang, S. Zhou, C.D. Ling, Z. Guo, Toward a Reversible Mn^{4+}/Mn^{2+} Redox Reaction and Dendrite-Free Zn Anode in Near-Neutral Aqueous Zn/MnO_2 Batteries via Salt Anion Chemistry, Adv. Energy Mater. 10 (2020) 1904163, https://doi.org/10.1002/aenm.201904163.
[12] L. Wu, Y. Dong, Recent progress of carbon nanomaterials for high-performance cathodes and anodes in aqueous zinc ion batteries, Energy Storage Mater. 41 (2021) 715–737, https://doi.org/10.1016/j.ensm.2021.07.004.
[13] Y.H. Zou, X.Z. Yang, L. Shen, Y.W. Su, Z.Y. Chen, X. Gao, J. Zhou, J.Y. Sun, Emerging strategies for steering orientational deposition toward high-performance Zn metal anodes, Energy Environ. Sci. 15 (2022) 5017–5038, https://doi.org/10.1039/d2ee02416k.
[14] J. Cao, D. Zhang, X. Zhang, Z. Zeng, J. Qin, Y. Huang, Strategies of regulating Zn^{2+} solvation structures for dendrite-free and side reaction-suppressed zinc-ion batteries, Energy Environ. Sci. 15 (2022) 499–528, https://doi.org/10.1039/d1ee03377h.
[15] H. He, H. Qin, J. Wu, X. Chen, R. Huang, F. Shen, Z. Wu, G. Chen, S. Yin, J. Liu, Engineering interfacial layers to enable Zn metal anodes for aqueous zinc-ion batteries, Energy Storage Mater. 43 (2021) 317–336, https://doi.org/10.1016/j.ensm.2021.09.012.
[16] F. Tao, Y. Liu, X. Ren, J. Wang, Y. Zhou, Y. Miao, F. Ren, S. Wei, J. Ma, Different surface modification methods and coating materials of zinc metal anode, J. Energy Chem. 66 (2022) 397–412, https://doi.org/10.1016/j.jechem.2021.08.022.
[17] C. Li, L. Wang, J. Zhang, D. Zhang, J. Du, Y. Yao, G. Hong, Roadmap on the protective strategies of zinc anodes in aqueous electrolyte, Energy Storage Mater. 44 (2022) 104–135, https://doi.org/10.1016/j.ensm.2021.10.020.
[18] C. Deng, X. Xie, J. Han, Y. Tang, J. Gao, C. Liu, X. Shi, J. Zhou, S. Liang, A Sieve-Functional and Uniform-Porous Kaolin Layer toward Stable Zinc Metal Anode, Adv. Funct. Mater. 30 (2020) 2000599, https://doi.org/10.1002/adfm.202000599.
[19] C. Li, X. Shi, S. Liang, X. Ma, M. Han, X. Wu, J. Zhou, Spatially homogeneous copper foam as surface dendrite-free host for zinc metal anode, Chem. Eng. J. 379 (2020), https://doi.org/10.1016/j.cej.2019.122248 122248.
[20] Y. Wang, Z. Wang, F. Yang, S. Liu, S. Zhang, J. Mao, Z. Guo, Electrolyte Engineering Enables High Performance Zinc-Ion Batteries, Small 18 (2022) 2107033, https://doi.org/10.1002/smll.202107033.
[21] S. Liu, J.P. Vongsvivut, Y. Wang, R. Zhang, F. Yang, S. Zhang, K. Davey, J. Mao, Z. Guo, Monolithic Phosphate Interphase for Highly Reversible and Stable Zn Metal Anode, Angew. Chem. Int. Ed. 62 (2023) e202215600.
[22] Y. Liu, T. Guo, Q. Liu, F. Xiong, M. Huang, Y. An, J. Wang, Q. An, C. Liu, L. Mai, Ultrathin ZrO_2 coating layer regulates Zn deposition and raises long-life performance of aqueous Zn batteries, Mater. Today Energy 28 (2022), https://doi.org/10.1016/j.mtener.2022.101056 101056.
[23] R. Wang, Q. Wu, M. Wu, J. Zheng, J. Cui, Q. Kang, Z. Qi, J. Ma, Z. Wang, H. Liang, Interface engineering of Zn meal anodes using electrochemically inert Al2O3 protective nanocoatings, Nano Res. 15 (2022) 7227–7233, https://doi.org/10.1007/s12274-022-4477-1.
[24] L. Dai, T. Wang, B. Jin, N. Liu, Y. Niu, W. Meng, Z. Gao, X. Wu, L. Wang, Z. He, γ-Al_2O_3 coating layer confining zinc dendrite growth for high stability aqueous rechargeable zinc-ion batteries, Surf. Coat. Technol. 427 (2021), https://doi.org/10.1016/j.surfcoat.2021.127813 127813.
[25] B. Li, B. Jin, R. Zhang, K. Ma, X. Wu, L. Dai, L. Wang, Z. He, Structural design and interfacial characteristics endow $NaTi_2(PO_4)_3$ coated zinc anode with high capacity and better cycling stability, Surf. Coat. Technol. 425 (2021), https://doi.org/10.1016/j.surfcoat.2021.127699 127699.
[26] B. Li, J. Xue, X. Lv, R. Zhang, K. Ma, X. Wu, L. Dai, L. Wang, Z. He, A facile coating strategy for high stability aqueous zinc ion batteries: Porous rutile nano-TiO2 coating on zinc anode, Surf. Coat. Technol. 421 (2021), https://doi.org/10.1016/j.surfcoat.2021.127367 127367.
[27] C. Mao, Y. Chang, X. Zhao, X. Dong, Y. Geng, N. Zhang, L. Dai, X. Wu, L. Wang, Z. He, Functional carbon materials for high-performance Zn metal anodes, J. Energy Chem. 75 (2022) 135–153, https://doi.org/10.1016/j.jechem.2022.07.034.
[28] Y. Su, X. Yang, Q. Zhang, J. Sun, Z. Liu, Carbon nanomaterials for highly stable Zn anode: Recent progress and future outlook, J. Electroanal. Chem. 904 (2022), https://doi.org/10.1016/j.jelechem.2021.115883 115883.
[29] Z. Li, L. Wu, S. Dong, T. Xu, S. Li, Y. An, J. Jiang, X. Zhang, Pencil Drawing Stable Interface for Reversible and Durable Aqueous Zinc-Ion Batteries, Adv. Funct. Mater. 31 (2020) 2006495, https://doi.org/10.1002/adfm.202006495.
[30] W. Li, K. Wang, M. Zhou, H. Zhan, S. Cheng, K. Jiang, Advanced Low-Cost, High-Voltage, Long-Life Aqueous Hybrid Sodium/Zinc Batteries Enabled by a Dendrite-Free Zinc Anode and Concentrated Electrolyte, ACS Appl. Mater. Interfaces 10 (2018) 22059–22066, https://doi.org/10.1021/acsami.8b04085.
[31] J. Zheng, Q. Zhao, T. Tang, J. Yin, C.D. Quilty, G.D. Renderos, X. Liu, Y. Deng, L. Wang, D.C. Bock, C. Jaye, D. Zhang, E.S. Takeuchi, K.J. Takeuchi, A.C. Marschilok, L.A. Archer, Reversible epitaxial electrodeposition of metals in battery anodes, Science 366 (2019) 645–648, https://doi.org/10.1126/science.aax6873.
[32] J. Zhou, M. Xie, F. Wu, Y. Mei, Y. Hao, R. Huang, G. Wei, A. Liu, L. Li, R. Chen, Ultrathin Surface Coating of Nitrogen-Doped Graphene Enables Stable Zinc Anodes for Aqueous Zinc-Ion Batteries, Adv. Mater. 33 (2021) 2101649, https://doi.org/10.1002/adma.202101649.
[33] A. Xia, X. Pu, Y. Tao, H. Liu, Y. Wang, Graphene oxide spontaneous reduction and self-assembly on the zinc metal surface enabling a dendrite-free anode for long-life zinc rechargeable aqueous batteries, Appl. Surf. Sci. 481 (2019) 852–859, https://doi.org/10.1016/j.apsusc.2019.03.197.
[34] Q. Yang, Y. Guo, B. Yan, C. Wang, Z. Liu, Z. Huang, Y. Wang, Y. Li, H. Li, L. Song, J. Fan, C. Zhi, Hydrogen-Substituted Graphdiyne Ion Tunnels Directing Concentration Redistribution for Commercial-Grade Dendrite-Free Zinc Anodes, Adv. Mater. 32 (2020) 2001755, https://doi.org/10.1002/adma.202001755.
[35] C. Wu, K. Xie, K. Ren, S. Yang, Q. Wang, Dendrite-free Zn anodes enabled by functional nitrogen-doped carbon protective layers for aqueous zinc-ion batteries, Dalton Trans. 49 (2020) 17629–17634, https://doi.org/10.1039/d0dt03459b.
[36] R. Yuksel, O. Buyukcakir, W.K. Seong, R.S. Ruoff, Metal-Organic Framework Integrated Anodes for Aqueous Zinc-Ion Batteries, Adv. Energy Mater. 10 (2020) 1904215, https://doi.org/10.1002/aenm.201904215.
[37] Y. Du, C. Liu, Y. Liu, Q. Han, X. Chi, Y. Liu, Carbon fiber micron film guided uniform plating/stripping of metals: A universal approach for highly stable metal batteries, Electrochim. Acta 339 (2020), https://doi.org/10.1016/j.electacta.2020.135867 135867.
[38] T. Jawhari, A. Roid, J. Casado, Raman spectroscopic characterization of some commercially available carbon black materials, Carbon 33 (11) (1995) 1561–1565.
[39] A. Sadezky, H. Muckenhuber, H. Grothe, R. Niessner, U. Pöschl, Raman microspectroscopy of soot and related carbonaceous materials: Spectral analysis and structural information, Carbon 43 (2005) 1731–1742, https://doi.org/10.1016/j.carbon.2005.02.018.
[40] K. Zhao, C. Wang, Y. Yu, M. Yan, Q. Wei, P. He, Y. Dong, Z. Zhang, X. Wang, L. Mai, Ultrathin Surface Coating Enables Stabilized Zinc Metal Anode, Adv. Mater. Interfaces 5 (2018) 1800848, https://doi.org/10.1002/admi.201800848.
[41] H.J. Kim, S. Kim, K. Heo, J.H. Lim, H. Yashiro, S.T. Myung, Nature of Zinc-Derived Dendrite and Its Suppression in Mildly Acidic Aqueous Zinc-Ion Battery, Adv. Energy Mater. 13 (2022) 2203189, https://doi.org/10.1002/aenm.202203189.
[42] W. Shi, Z. Song, J. Wang, Q. Li, Q. An, Phytic acid conversion film interfacial engineering for stabilizing zinc metal anode, Chem. Eng. J. 446 (2022), https://doi.org/10.1016/j.cej.2022.137295 137295.
[43] J. Hao, B. Li, X. Li, X. Zeng, S. Zhang, F. Yang, S. Liu, D. Li, C. Wu, Z. Guo, An In-Depth Study of Zn Metal Surface Chemistry for Advanced Aqueous Zn-Ion Batteries, Adv. Mater. 32 (2020) 2003021, https://doi.org/10.1002/adma.202003021.
[44] F. Ming, H. Liang, Y. Lei, S. Kandambeth, M. Eddaoudi, H.N. Alshareef, Layered $Mg_xV_2O_5{\cdot}nH_2O$ as Cathode Material for High-Performance Aqueous Zinc Ion Batteries, ACS Energy Lett. 3 (2018) 2602–2609, https://doi.org/10.1021/acsenergylett.8b01423.

Supplementary Information

Stable zinc metal anode with an ultrathin carbon coating for zin-ion batteries

Xiaolin Zhang, Qingdong Ruan, Liangliang Liu, Dan Li, Yue Xu, Chao Huang, Fangyu Xiong,* Bin Wang,* and Paul K Chu*

Department of Physics, Department of Materials Science and Engineering, and Department of Biomedical Engineering, City University of Hong Kong, Tat Chee Avenue, Kowloon, Hong Kong, China

* **Corresponding Authors**: fxiong@cityu.edu.hk (F. Xiong), bwang63@cityu.edu.hk (B. Wang), paul.chu@cityu.edu.hk (P.K. Chu)

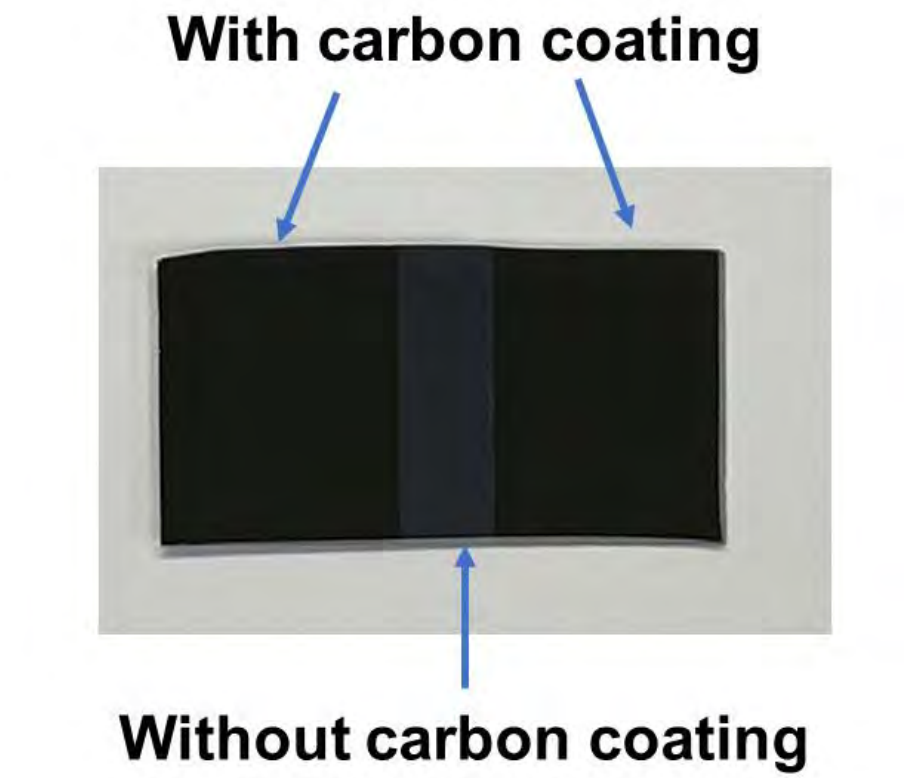

Fig. S1. Photograph of the carbon coating deposited on Si.

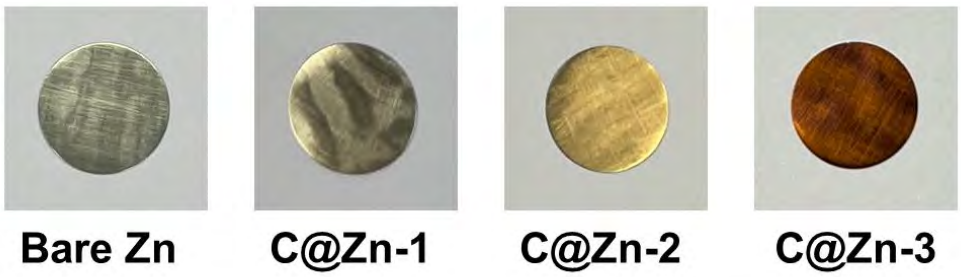

Fig. S2. Photographs of bare Zn, C@Zn-1, C@Zn-2, and C@Zn-3.

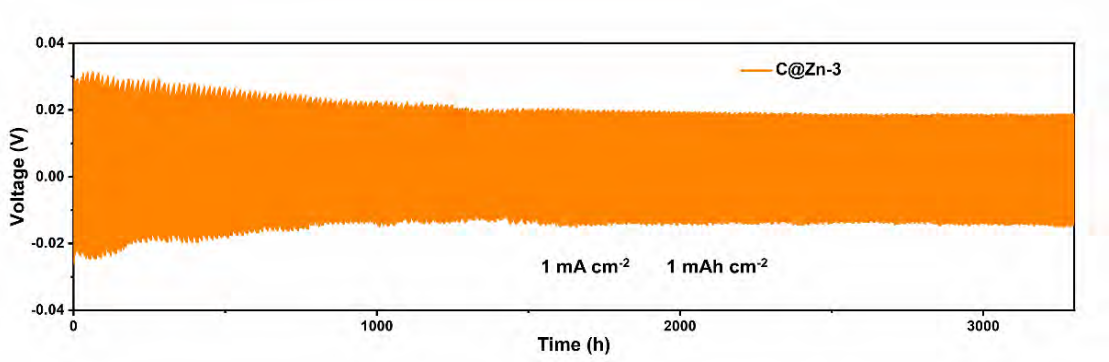

Fig. S3. Cycling voltage profiles of the C@Zn-3 symmetrical cell at 1 mA cm^{-2} with an areal capacity of 1 mA h cm^{-2}.

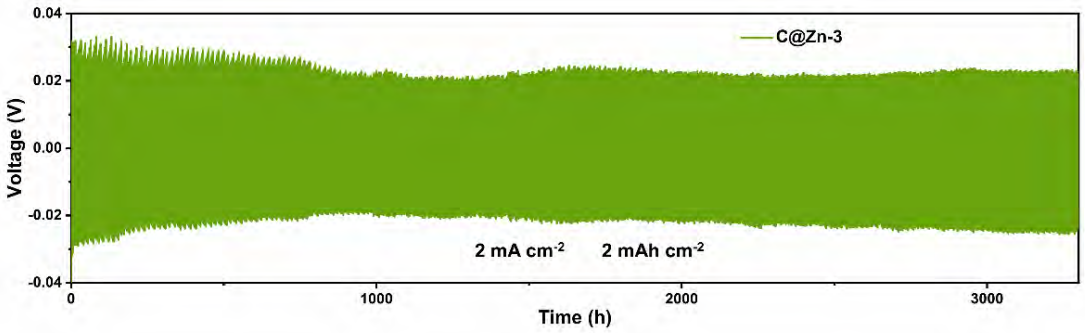

Fig. S4. Cycling voltage profiles of the C@Zn-3 symmetrical cell at 2 mA cm^{-2} with an areal capacity of 2 mA h cm^{-2}.

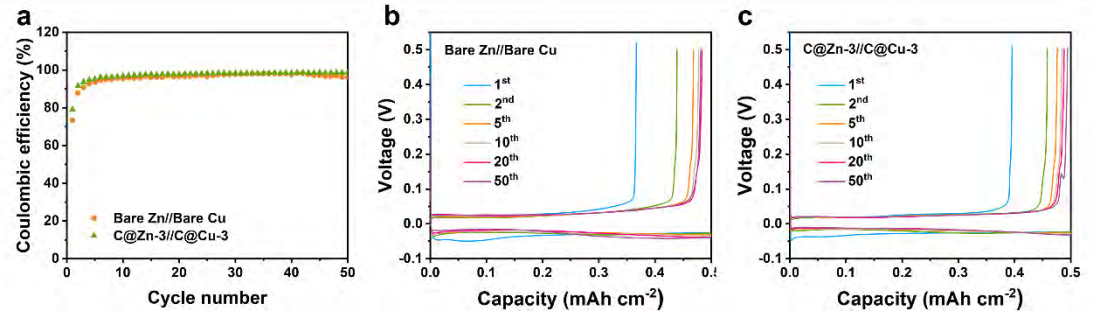

Fig. S5. (a) Coulombic efficiency versus cycle number profiles of bare Zn//bare Cu and C@Zn-3//C@Cu-3 cells at 0.5 mA cm^{-2} and 0.5 mAh cm^{-2}; Voltage profiles of (b) Bare Zn//bare Cu and (c) C@Zn-3//C@Cu-3 cells at 0.5 mA cm^{-2} and 0.5 mAh cm^{-2}.

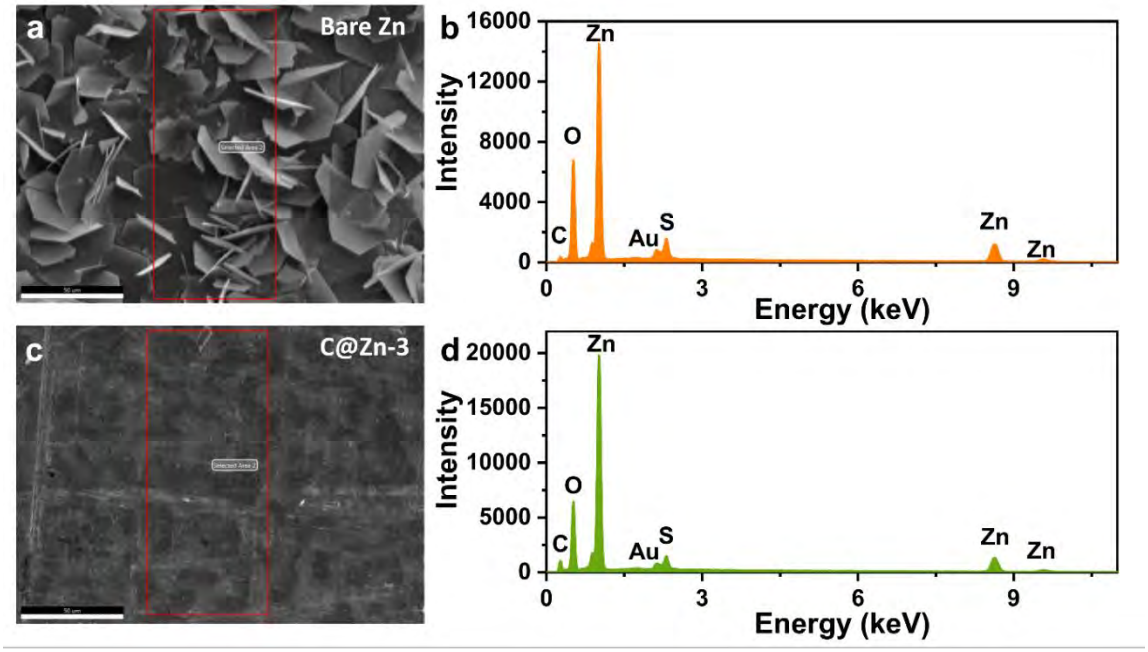

Fig. S6. (a) SEM image and (b) EDS spectrum of bare Zn after soaking in 2 M $ZnSO_4$ for 3 days; (c) SEM image and (d) EDS spectrum of C@Zn-3 after soaking in 2 M $ZnSO_4$ for 3 days.

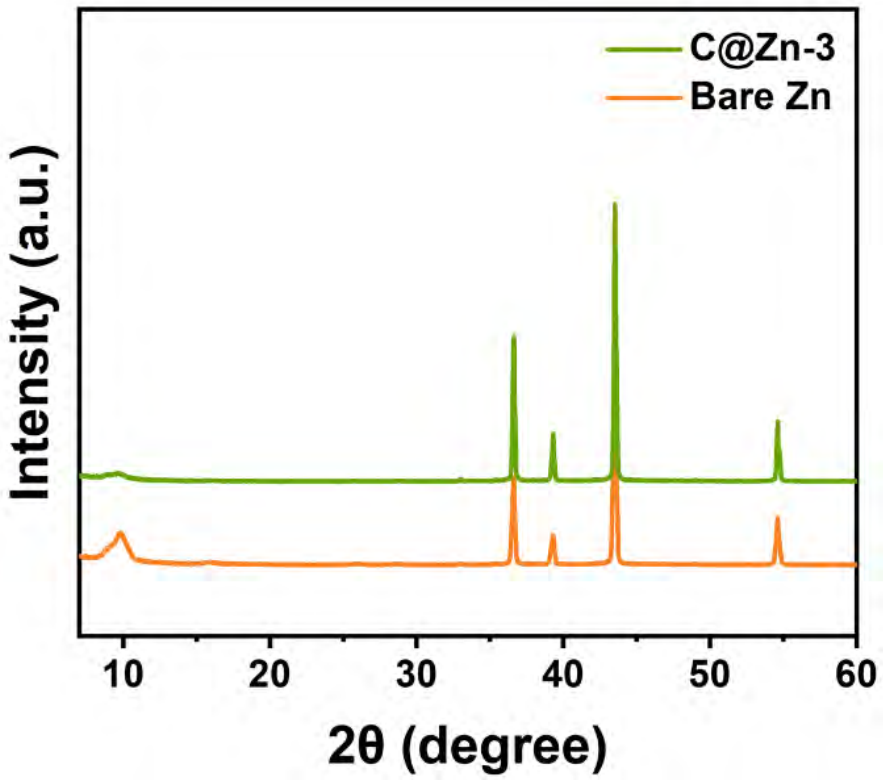

Fig. S7. XRD patterns of the bare Zn and C@Zn-3 anodes after 20 plating/stripping cycles at 0.5 mA cm^{-2} and 0.5 mAh cm^{-2}.

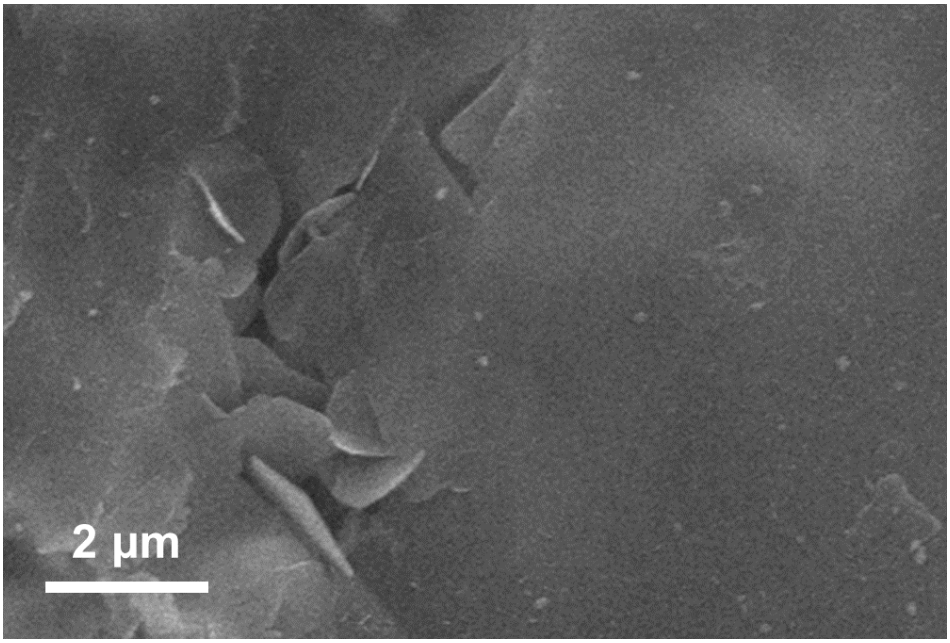

Fig. S8. SEM image of the C@Zn-3 anode after Zn plating at 0.5 mA cm^{-2} for 1 h.

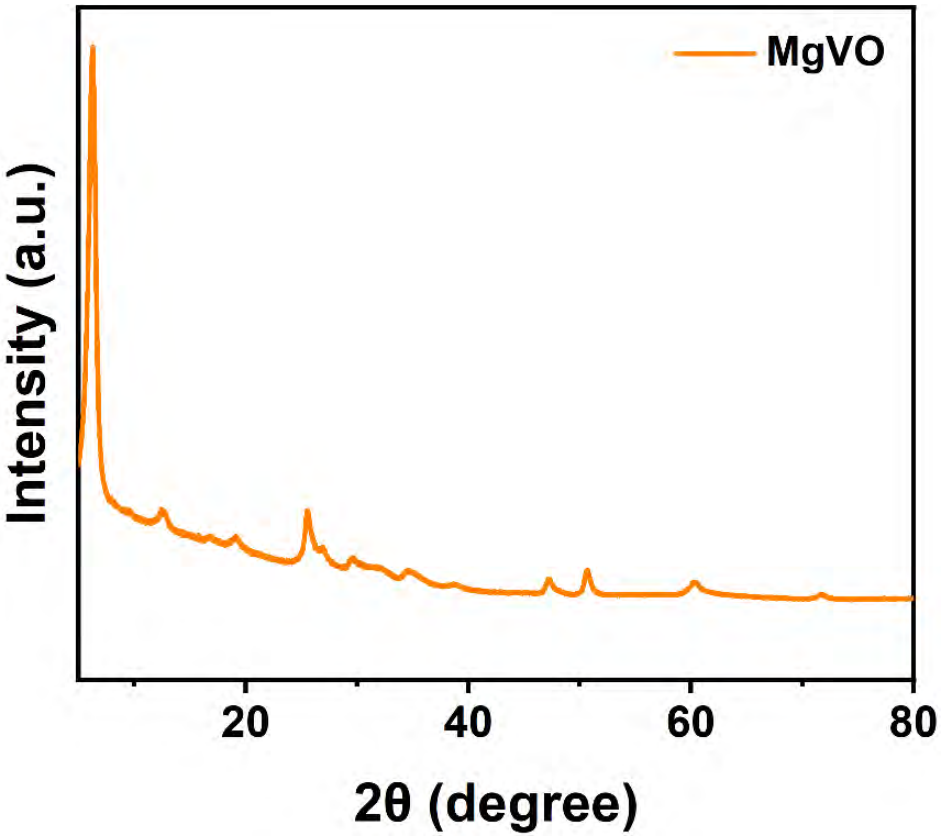

Fig. S9. XRD pattern of $Mg_xV_2O_5 \cdot nH_2O$.

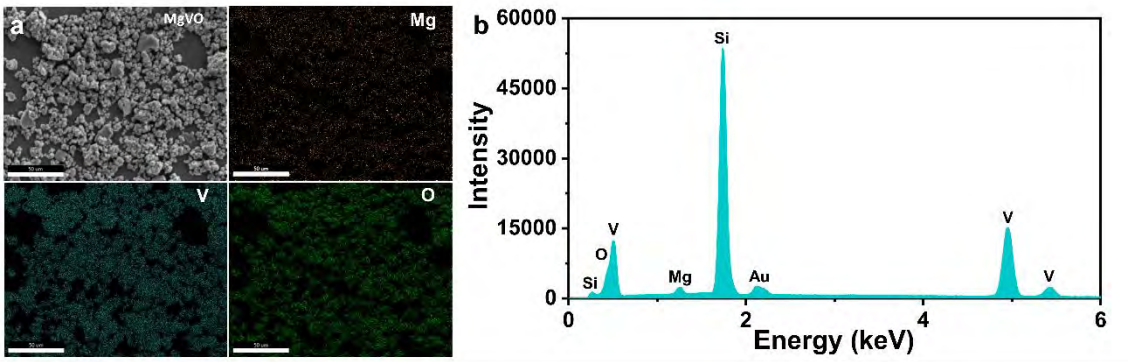

Fig. S10. (a) EDS elemental maps and (b) EDS spectrum of $Mg_xV_2O_5 \cdot nH_2O$ (Si signal originating from the substrate).

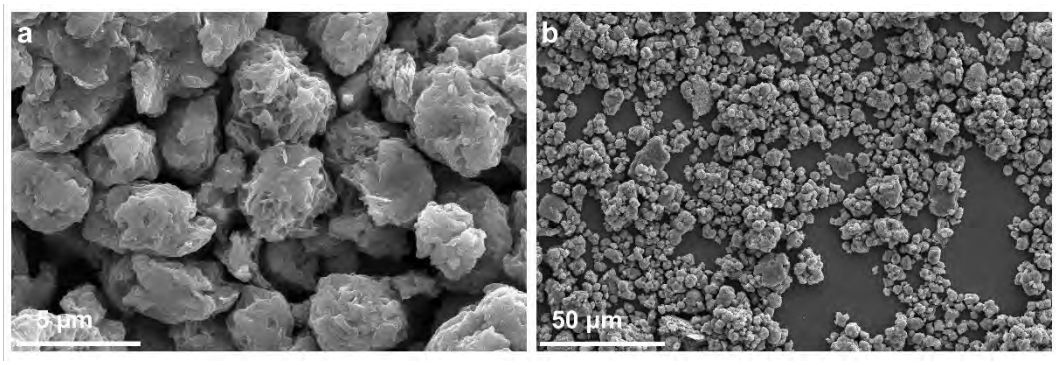

Fig. S11. SEM images of $Mg_xV_2O_5 \cdot nH_2O$.

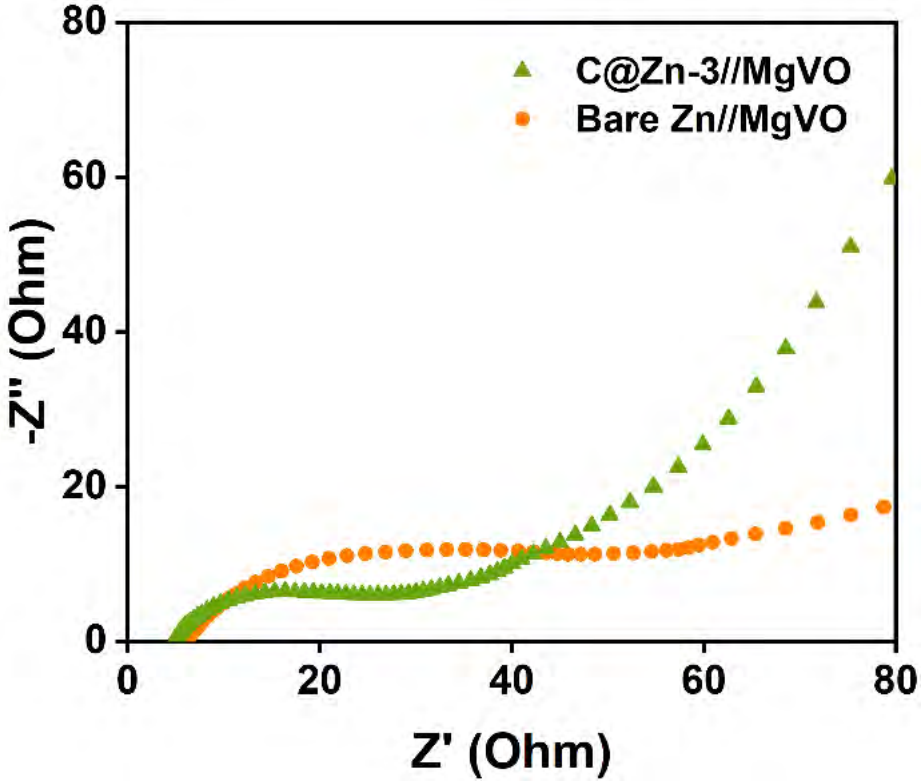

Fig. S12. EIS plots of C@Zn-3//MgVO and bare Zn//MgVO batteries.